Zebrafish *trilobite* identifies new roles for Strabismus in gastrulation and neuronal movements

Jason R. Jessen*, Jacek Topczewski*, Stephanie Bingham†, Diane S. Sepich*, Florence Marlow*, Anand Chandrasekhar† and Lilianna Solnica-Krezel*‡

**Department of Biological Sciences, Vanderbilt University, VU Station B 351634, Nashville, TN 37235, USA*
†Division of Biological Sciences, University of Missouri, Columbia, MO 65211, USA
‡e-mail: lilianna.solnica-krezel@vanderbilt.edu.

Published online: July 8 2002; DOI:10.1038/ncb828

Embryonic morphogenesis is driven by a suite of cell behaviours, including coordinated shape changes, cellular rearrangements and individual cell migrations, whose molecular determinants are largely unknown. In the zebrafish, *Dani rerio*, *trilobite* mutant embryos have defects in gastrulation movements[1–4] and posterior migration of hindbrain neurons[5]. Here, we have used positional cloning to demonstrate that *trilobite* mutations disrupt the transmembrane protein Strabismus (Stbm)/Van Gogh (Vang), previously associated with planar cell polarity (PCP) in *Drosophila melanogaster*[6,7], and PCP and canonical Wnt/β-catenin signalling in vertebrates[8,9]. Our genetic and molecular analyses argue that during gastrulation, *trilobite* interacts with the PCP pathway without affecting canonical Wnt signalling. Furthermore, *trilobite* may regulate neuronal migration independently of PCP molecules. We show that *trilobite* mediates polarization of distinct movement behaviours. During gastrulation convergence and extension movements, *trilobite* regulates mediolateral cell polarity underlying effective intercalation and directed dorsal migration at increasing velocities. In the hindbrain, *trilobite* controls effective migration of branchiomotor neurons towards posterior rhombomeres. Mosaic analyses show *trilobite* functions cell-autonomously and non-autonomously in gastrulae and the hindbrain. We propose Trilobite/Stbm mediates cellular interactions that confer directionality on distinct movements during vertebrate embryogenesis.

To determine the molecular underpinnings of various cell movements in vertebrate embryos, we undertook a molecular characterization of the *trilobite* (*tri*) locus[1,4]. Through positional cloning, we identified a *stbm*/*vang* homologue[9], a gene that is broadly expressed during early development[9], as a candidate for *tri* (see Supplementary Information, Fig. S1). Analysis of the tri^{m209}, tri^{m747}, tri^{tc240a} and tri^{tk50f} chemically-induced alleles[10,11] demonstrated that each contains a disruption in *stbm* (Fig. 1a). In tri^{m747}, a nonsense mutation at Ser 427 is predicted to shorten Stbm by 93 amino acids. The tri^{m209} allele harbours a 13 base pair insertion of intronic sequence, resulting in a frameshift at Ala 441 and premature termination of translation. The tri^{tc240a} allele carries a 39 base pair insertion, resulting in the in-frame addition of 13 amino acids at Arg 21. Transcripts for *stbm* were not detected in tri^{tk50f} homozygous mutant embryos and genomic PCR indicated that at least part of the coding sequence is deleted (data not shown). To confirm that *stbm* represents the *tri* gene, we injected *stbm* RNA into embryos produced by *tri* heterozygous parents and scored its effect on the mutant phenotype. Partial suppression of the convergence and extension defect was observed in all mutant embryos ($n = 75$) at 1 day post-fertilization (Fig. 1b–d). In contrast, mutated *stbm* RNA encoded by the tri^{m747} allele did not affect wild-type or *tri* phenotypes (data not shown), suggesting this is a loss-of-function and likely a null mutation. A hallmark of genes controlling tissue or planar cell polarity (PCP) is that their increased activity also impairs gastrulation[8,12–14]. Overexpression of *stbm* RNA in wild-type embryos strongly inhibited convergence and extension, as indicated by shorter embryonic axes, synopthalmia, and dorsal flexure (Fig. 1e), effects resembling interference with Dishevelled (Dsh) function[12] and *tri* mutant phenotypes[1,4]. In loss-of-function experiments, injection of *stbm* antisense morpholino (MO) oligonucleotides[15] caused a modest convergence and extension defect in 95% of wild-type embryos ($n = 374$; Fig. 1f), consistent with previous experiments in zebrafish[9] and *Xenopus laevis*[8]. Injection of *stbm* MO into *tri* embryos enhanced the convergence and extension defect, suggesting that maternally-derived *tri* (ref. 9) influences gastrulation movements (Fig. 1g). Moreover, the *tri* motor neuron migration defect was also phenocopied by injection of *stbm* MO into wild-type embryos (62%, $n = 262$; Fig. 1h–j). Conversely, injection of *stbm* RNA into *tri* embryos frequently restored wild-type motor neuron migration (33%, $n = 43$; Fig. 1k–m). Together, these results establish that genetic lesions in a zebrafish *stbm* homologue cause the *tri* phenotype and hereafter we will refer to this gene as *tri*.

In *Drosophila*, *stbm*/*vang* is instructive during the establishment of cell fates within ommatidia[6,7] and genetically interacts with the PCP pathway to establish wing tissue polarity[6]. In vertebrates, Stbm/Vang was proposed to function downstream of Wnt and Frizzled to activate the PCP pathway while antagonizing canonical Wnt/β-catenin signalling, and thus anteroposterior neural patterning[16]. However, there are conflicting reports that argue for and against an involvement of mouse, fish and frog *stbm* in neural patterning[8,9,17,18]. Previous analyses of *tri* phenotypes did not identify anteroposterior neural patterning defects[1–5], a conclusion we have extended here for simultaneous interference with maternal and zygotic *tri* functions (Supplementary Information, Fig. S2). Given the evidence implicating canonical Wnt signalling as the key regulator of anteroposterior neural patterning in vertebrates[19–21], we argue that Tri/Stbm is neither required nor capable of significantly modulating canonical Wnt signalling in zebrafish gastrulae[9,18].

With regard to the PCP pathway, genetic epistasis experiments identified functional interactions between *tri* and *silberblick* (*slb*/*wnt11*)[22] and *knypek* (*glypican 4/6*)[3] PCP signalling mutants,

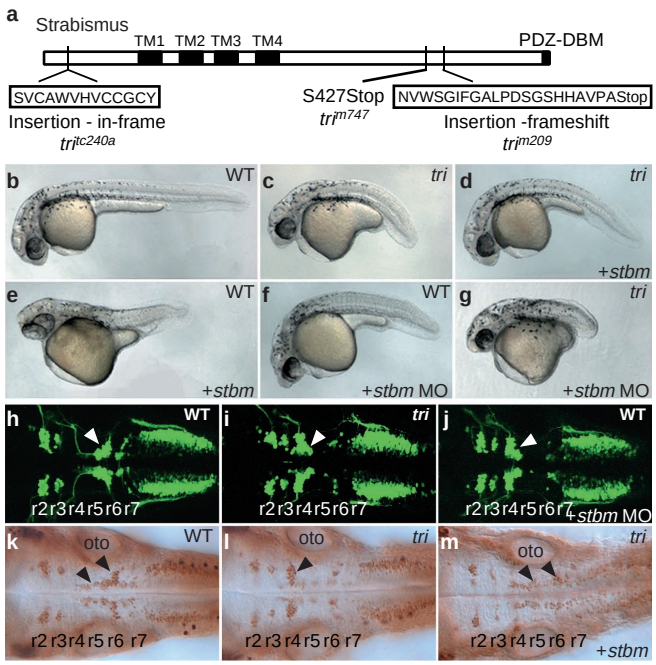

Figure 1 ***tri* encodes a Stbm homologue. a**, A schematic representation of Stbm, showing mutations in three *tri* alleles (TM, putative transmembrane domains; PDZ-DBM, putative PDZ-domain binding motif). **b**–**g**, Stbm controls convergence and extension cell movements. Wild-type (**b**) and tri^{m209} (**c**) embryos at 1 day post-fertilization. Injection of *stbm* RNA partially suppresses the *tri* convergence and extension defect (**d**). Wild-type embryos injected with *stbm* RNA (**e**) or *stbm* MO (**f**) show inhibited convergence and extension. **g**, *stbm* MO enhances the convergence and extension defect in *tri* mutant embryos. **h**–**j**, *stbm* MO phenocopies *tri* neuronal migration phenotype. Embryos at 36 h post-fertilization with *gfp* expression in branchiomotor neurons under control of the *islet1* promoter (dorsal views). Motor neurons (arrowheads) induced in rhombomere 4 (r4) migrate into r6 and r7 in wild-type (**h**) but remain in r4 in tri^{m209} embryos (**i**) and wild-type embryos injected with *stbm* MO (**j**). **k**–**m**, Stbm suppresses *tri* neuronal migration defect. Embryos at 36 h post-fertilization with anti-Islet antibody-labelled branchiomotor neurons. Motor neurons migrated into r6 in wild-type (**k**) and tri^{m209} embryos injected with *stbm* RNA (**m**), but not in tri^{m209} (**l**) embryos. oto, otocyst.

Table 1 Mediolateral elongation of ectodermal cells requires autonomous and non-autonomous *tri* function

Genotype		LWR	MLA	cells/
Donor	Host		(% ± 20°)	embryos (*n*)
WT*		1.85 ± 0.56	73	274/4
*tri**		1.51 ± 0.31[a]	27[e]	142/4
WT	WT	1.83 ± 0.58[b]	66[f]	47/3
WT	*tri*	1.51 ± 0.33[c]	37[g]	91/7
tri	WT	1.50 ± 0.31[d]	30[h]	116/4

*control embryos
[a]vs. WT, significantly different at $P < 0.0001$
[b]vs. WT, not significantly different at $P > 0.5$
[c]vs. WT, $P < 0.0001$; vs. *tri*, $P > 0.5$
[d]vs. WT, $P < 0.0001$; vs. *tri*, $P > 0.5$
[e]vs. WT, significantly different at $P < 0.0001$
[f]vs. WT, $P > 0.5$
[g]vs. WT, $P < 0.0001$; vs. *tri*, not significantly different at $P > 0.1$
[h]vs. WT, $P < 0.0001$; vs. *tri*, $P > 0.5$

suggesting they function in the same or parallel pathways during convergence and extension. However, we were unable to suppress the *tri* convergence and extension defect by injecting either *dsh-ΔN* or *rho kinase 2* RNAs (Supplementary Information, Fig. S3), downstream mediators of PCP signalling that are capable of suppressing *slb* gastrulation defects[13,23]. Moreover, neither excess *tri* function, nor its reduction with MOs could suppress the slb^{tz216} gastrulation mutant phenotype (Supplementary Information, Fig. S3). We next showed that although overexpression of *tri* did not alter the intracellular distribution of Rho kinase 2 (ref. 23), it did interfere with the ability of excess Wnt11 to do so (Supplementary Information, Fig. S3). Together, these results suggest Tri/Stbm can modulate PCP signalling, but that it is not simply a positive or negative component of a linear PCP pathway.

Although interference with Tri/Stbm function inhibits convergence and extension in fish and frogs[2,8,9], the cellular basis of this defect is unknown. We asked whether *tri* mediates mediolateral cell elongation, a behaviour critical for cell intercalations underlying convergence and extension movements in the dorsal regions of late zebrafish gastrulae[24,25] and dependent on PCP pathway components[23,26,27]. Using confocal microscopy, we demonstrated that the length-to-width ratio (LWR) of paraxial ectodermal cells is reduced in *tri* gastrulae, compared to wild type (Fig. 2a–d and Table 1). The mediolateral alignment (MLA) of paraxial ectodermal cells is also reduced in *tri* embryos (Fig. 2a,e and Table 1). To test the cell-autonomy of *tri* function in convergence and extension, we performed transplantations at the blastula stage and assessed the morphology of donor-derived paraxial ectodermal cells at late gastrulation. Wild-type cells transplanted into wild-type hosts were elongated and mediolaterally aligned (Fig. 2d,e and Table 1). In *tri* hosts, wild-type cells were rounded and showed no mediolateral bias (Fig. 2d–f and Table 1). Labelled *tri* cells also did not elongate or mediolaterally align in wild-type hosts (Fig. 2d,e,g and Table 1). The lack of elongation and alignment of wild-type and *tri* donor-derived ectodermal cells was similar to that observed for *tri* mutant ectodermal cells (Table 1). The inability of *tri* cells to behave normally in a wild-type environment indicates that *tri* functions autonomously in cell polarization. Moreover, failure of wild-type cells to elongate and mediolaterally align in *tri* embryos demonstrates that *tri* function also has a non-autonomous component. Therefore, as proposed for *Drosophila* Stbm/Vang[14], Tri/Stbm seems to influence intercellular communication that is essential for the establishment of tissue polarity during gastrulation.

In zebrafish gastrulae, lateral mesodermal and ectodermal cell populations move dorsally at increasing speed[2,24] (Fig. 3a). The acceleration of convergence movements is compromised in *tri* mutant embryos[2]. We used time-lapse Nomarski imaging to identify specific cell behaviours underlying the increased rates of dorsal convergence and asked whether these behaviours require *tri* function. At mid-gastrulation, we observed that wild-type lateral mesodermal cells are not elongated and migrate as individuals with a slow net dorsal speed along indirect paths (Fig. 3b–d and Table 2). At this stage, the morphology and behaviour of *tri* cells does not differ from wild type (Fig. 3b,c,e and Table 2). By late gastrulation, wild-type mesodermal cells are significantly more elongated and migrate dorsally at increased net speeds with more direct trajectories (Fig. 3b,c,f and Table 2; see also Supplementary Information, Movie S1). By contrast, late gastrulation *tri* cells are more rounded and move with a significantly reduced net dorsal speed along less direct trajectories when compared with their wild-type counterparts (Fig. 3b,c,g and Table 2; see also Supplementary Information, Movie S2). Although increasing rates of convergence have been observed in gastrulae of the teleost fish, *Fundulus heteroclitus*[28], the mediolateral lengthening of zebrafish lateral mesodermal cells associated with their increased net dorsal velocities represents a new behaviour. We propose that *tri*-dependent mediolateral cell polarization is required for persistent dorsal migration of cells along straight paths and consequently for the increased velocities of their convergence movements.

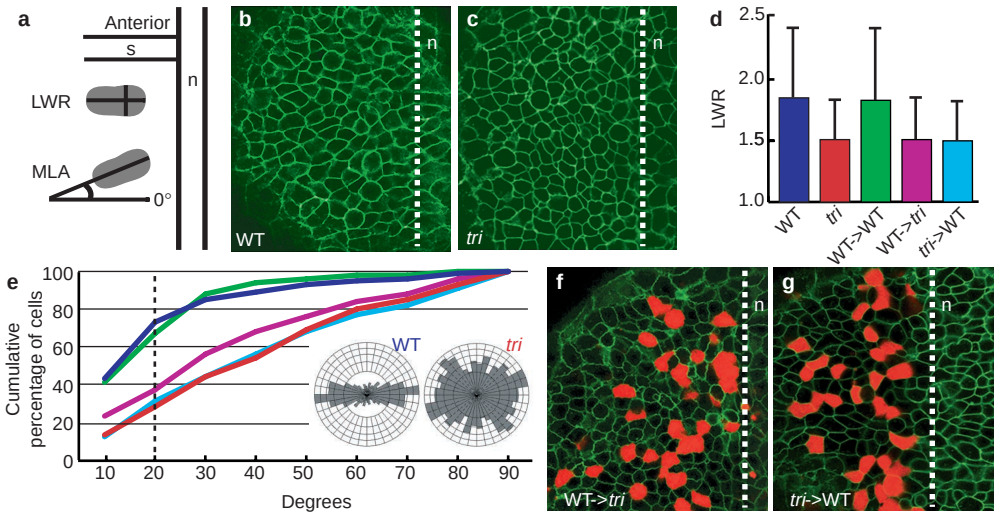

Figure 2 ***tri* functions autonomously and non-autonomously to control cell polarity. a**, A schematic representation of the methods used to measure cell elongation (LWR) and mediolateral alignment (MLA) relative to the notochord (n). Wild-type (**b**) and *tri* (**c**) ectodermal cells labelled with membrane-localized GFP (green). **d**, LWRs of wild-type and *tri* paraxial ectodermal cells and donor cells (wild-type->wild-type; wild-type->*tri*; *tri*->wild-type) with their standard deviations. **e**, Cumulative percentage of mediolaterally aligned paraxial ectodermal cells as a function of their angle, relative to a line perpendicular to the notochord. Graph line colours correspond to bar graph colours in **d**. Dashed line indicates sector ± 20° perpendicular to the notochord[27]. Rose diagrams (insets) depict cell orientations in wild-type and *tri* paraxial ectoderm of late gastrulae. The mediolateral axis corresponds to the horizontal plane (0°), perpendicular to the notochord, and the anteroposterior axis is aligned vertically (90°). Transplanted wild-type (**f**) and *tri* (**g**) donor-derived ectodermal cells (red) surrounded by host ectoderm (green) are shown. The dashed lines in **b**,**c**,**f** and **g** indicate notochord boundary. s, somite.

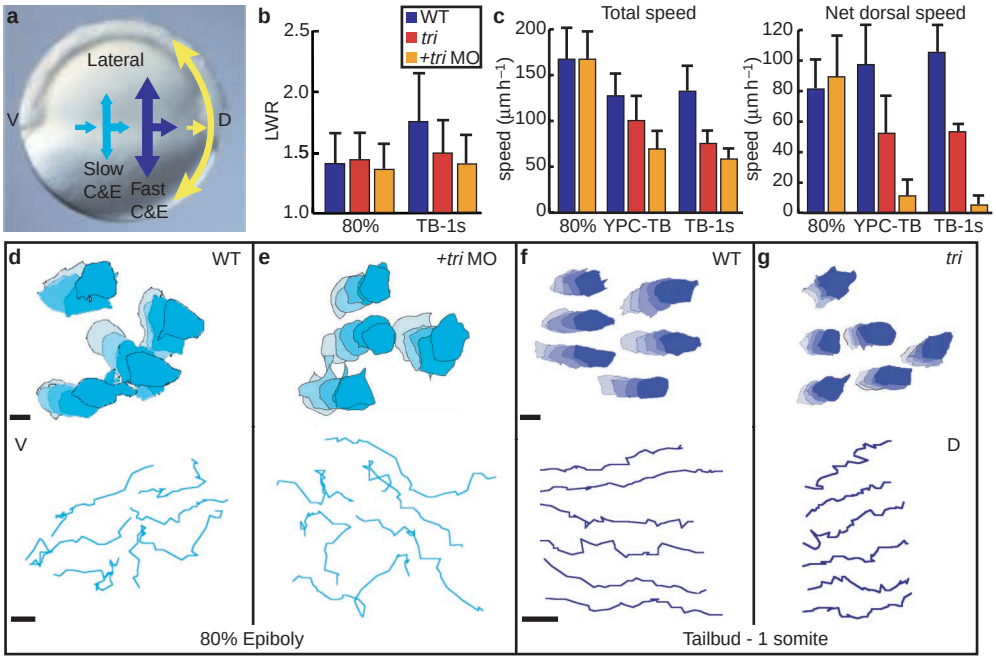

Figure 3 ***tri* is required for the increased net speed of directed dorsal migration. a**, Domains of convergence and extension cell movements in zebrafish gastrulae[24]. Yellow arrows in dorsal region indicate strong extension movements with little convergence. Light and dark blue arrows indicate domains of slow and fast convergence and extension, respectively. **b**, LWR of lateral mesodermal cells in wild-type and *tri* embryos, and *tri* embryos injected with *tri* MO. **c**, Total and net dorsal migration speeds of lateral mesodermal cells at 80% epiboly, yolk-plug closure (YPC)-tailbud (TB), and TB-1 somite stages. **d–g,** Shape changes and dorsal migration trajectories of lateral mesodermal cells. Colours match domains of slow and fast convergence and extension movement in **a**. D, dorsal. V, ventral. Scale bars represent 10 μm.

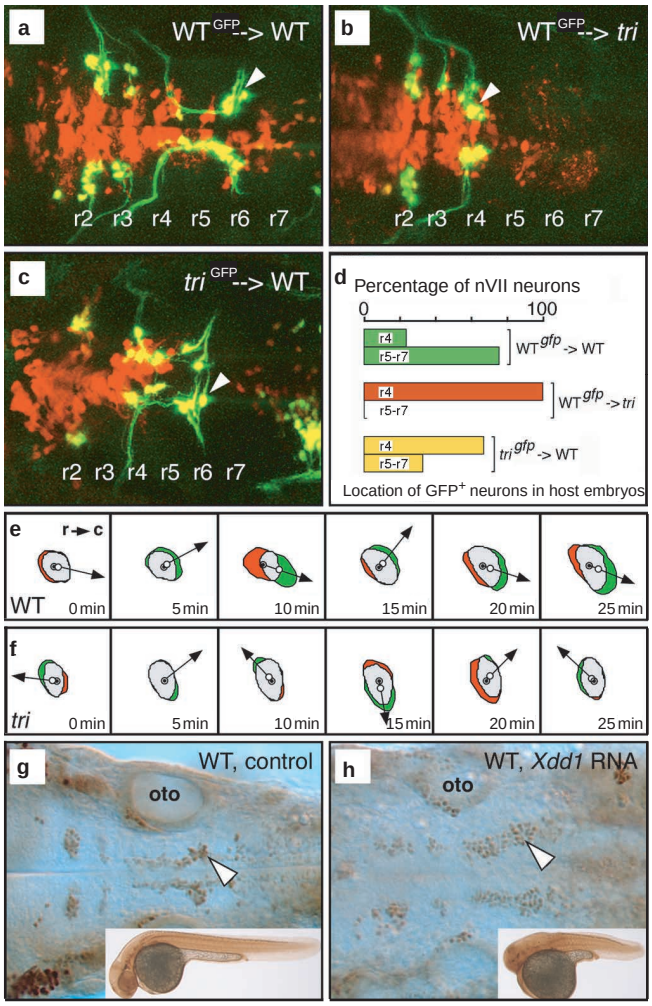

Figure 4 ***tri* functions autonomously and non-autonomously during tangential neuronal migration. a–c**, Dorsal views of hindbrain in unlabelled host embryos containing transplanted rhodamine–dextran-labelled donor cells (red), some of which differentiated into *GFP*-expressing motor neurons (green/yellow). Wild-type motor neurons (arrowhead) migrated out of r4 and into r6 in a wild-type host (**a**), but not in a tri^{tc240a} host (**b**). tri^{tc240a} motor neurons (arrowhead) migrated into r6 in a wild-type host (**c**). **d,** A quantitative summary of the transplantation data. **e**,**f**, Representative behaviours of wild-type and tri^{tc240a} motor neurons during a 25-min time-lapse recording. Red indicates area of retraction from previous cell position (closed circle marks cell centre) and green indicates area of expansion in current cell position (open circle marks cell centre). Arrows point in direction of cell movement. r, rostral; c, caudal. **e**, Wild-type motor neurons show biased caudal migration. **f**, tri^{tc240a} motor neurons meander showing no directionality. **g**,**h**, Dorsal views of wild-type hindbrains labelled with an Islet antibody. Motor neurons migrated into r6, posterior to the otocyst (oto), in control wild-type embryos (inset; **g**) and in *Xdd1*-injected wild-type embryos (**h**) showing a strong convergence and extension defect (inset).

Similar to the movements of lateral gastrula cells, facial (nVII) hindbrain branchiomotor neurons undergo directed migration from rhombomere 4 (r4) into r6 and r7 (refs 29,30). In *tri* mutant embryos, motor neurons induced in r4 fail to migrate tangentially into more posterior rhombomeres (see Supplementary Information, Movies S3 and S4), whereas radial migration of the motor neurons is unaffected[5]. We used mosaic analysis[31] to ask whether *tri* functions cell-autonomously in this process. About 75% of wild-type motor neurons migrated normally out of r4 into r6 and r7 after transplantation into wild-type hosts ($n = 175$ cells, 22 embryos; Fig. 4a,d). In contrast, wild-type motor neurons failed to migrate out of r4 in *tri* hosts ($n = 66$ cells, 11 embryos; Fig. 4b,d), identifying a non-cell-autonomous role for *tri* in the surrounding hindbrain tissue. In the reciprocal experiment, 33% of *tri* motor neurons migrated normally into r6 and r7 in wild-type hosts ($n = 90$ cells, 12 embryos; Fig. 4c,d) indicating that the *tri* phenotype can be rescued by the wild-type environment. However, as a high percentage of *tri* motor neurons failed to migrate in the wild-type environment, we suggest that *tri* function also has a cell-autonomous component during tangential migration of hindbrain motor neurons. Cumulatively, these experiments indicate that Tri/Stbm is required for cellular interactions that mediate migratory events in the gastrula and hindbrain.

We used time-lapse analysis of green fluorescent protein (GFP)-expressing nVII motor neurons to identify the cellular basis of the neuronal migration defect[5]. Whereas wild-type and *tri* neurons have similar LWRs (wild-type = 1.5 ± 0.2, $n = 9$; tri = 1.6 ± 0.3, $n = 10$; $p = 0.32$), *tri* neurons move slower (wild-type = $19.4 \pm 6.7\ \mu m\ h^{-1}$, $n = 9$; *tri* = $11.9 \pm 2.5\ \mu m\ h^{-1}$, $n = 10$; $p = 0.01$) and in random directions. Further analyses demonstrated that wild-type cells have caudally-biased expansion and rostrally-biased retraction zones (Fig. 4e), resulting in effective caudal translocation of cell bodies. In contrast, expansion and retraction zones form randomly around the periphery of *tri* neurons (Fig. 4f), producing insignificant caudal movement (wild-type = $11.3 \pm 9.3\ \mu m\ h^{-1}$, $n = 9$; *tri* = $1.6 \pm 3.2\ \mu m\ h^{-1}$, $n = 10$; $p = 0.02$). As dynamic changes in cell area are similar between wild-type and *tri* neurons (wild-type = $3.5 \pm 0.8\ \mu m^2 min^{-1}$, $n = 9$; *tri* = $3.1 \pm 0.9\ \mu m^2 min^{-1}$, $n = 10$; $p = 0.32$), we propose that *tri* neurons either cannot stabilize their protrusions or cannot polarize their orientation. Interestingly there is strong expression of *Ltap*, the mouse *stbm* homologue most similar to *tri*, in hindbrain r4 (ref. 32), suggesting a possible role for the mouse protein in tangential motor neuron migration. Taken together, our studies suggest that Tri/Stbm confers directionality on both gastrula and tangential neuronal cell migration.

Previously, it was shown that disruption of *knypek* (*glypican 4/6*), a positive modulator of PCP signalling that is broadly expressed in zebrafish embryos at the time of motor neuron migration[27], had no effect on tangential migration of motor neurons[5]. This suggested that these movements may occur independently of PCP signalling. Consistently, facial (nVII) motor neurons migrate normally in *slb* (*wnt11*; $n = 19$) and *pipetail* (*wnt5a*; $n = 53$) mutant embryos (data not shown). As Tri/Stbm can bind to Dsh *in vitro*[9], we examined motor neuron migration in wild-type embryos expressing Xdd1, a PCP-specific dominant-negative Dsh[12]. Ubiquitous overexpression of Myc-tagged *xdd1* in zebrafish embryos through 1-day post-fertilization caused severe convergence and extension defects that are consistent with previous results[13], but did not impair neuronal migration ($n = 77$; Fig. 4g,h and data not shown). Similarly, although *tri* expression can rescue neuronal migration in *tri* mutant embryos, *tri* overexpression in wild-type embryos caused severe convergence and extension defects without affecting motor neuron migration ($n = 54$; data not shown). These results suggest that Tri/Stbm may control tangential migration of hindbrain neurons through a Dsh-independent pathway distinct from non-canonical Wnt signalling.

It is noteworthy that Tri/Stbm has been employed by vertebrate embryos to control mediolateral intercalation during gastrulation and such distinct movement behaviours as directed migration of gastrula cells and hindbrain motor neurons. One question is whether there is a common role for Tri/Stbm in the regulation of these distinct cell behaviours. During gastrulation, *tri* function is required for cell polarization associated with intercalation and directed migration at increasing velocities. By contrast, migrating motor neurons do not exhibit an elongated morphology. However, in the absence of *tri* function, gastrula cells are unable to converge dorsally along straight trajectories and motor

Table 2 The net dorsal migration speed of wild-type lateral mesodermal cells increases as cells become mediolaterally elongated.

Genotype	Stage	LWR	Cells/embryos (*n*)	Total speed (μm h^{-1})	Net dorsal speed (μm h^{-1})	Cells/embryos (*n*)
WT	80%	1.40 ± 0.28	182/4	168 ± 41	81 ± 21	209/6
tri	80%	1.45 ± 0.26[a]	103/2	–	–	–
tri+MO	80%	1.34 ± 0.25[b]	100/2	168 ± 30	89 ± 30[f]	62/2
WT	TB-1s	1.74 ± 0.45[c]	402/13	133 ± 25	105 ± 22[g]	32/2
tri	TB-1s	1.50 ± 0.33[d]	88/2	76 ± 8	53 ± 6[h]	22/1
tri+MO	TB-1s	1.40 ± 0.26[e]	28/1	159 ± 12	5 ± 7	21/1

[a]vs. WT at 80%, not significantly different at $P > 0.2$
[b]vs. WT at 80%, not significantly different at $P > 0.07$
[c]vs. WT at 80%, significantly different at $p < 0.0001$
[d]vs. WT at TB-1s, $P < 0.0001$
[e]vs. WT at TB-1s, $P < 0.0001$
[f]vs. WT at 80%, not significantly different at $P > 0.3$
[g]vs. WT at 80%, $P < 0.0001$
[h]vs. WT at TB-1s, $P < 0.0001$

neurons move their cell bodies in random directions, rather then exclusively towards posterior rhombomeres. We propose that Tri/Stbm confers directionality on cell intercalation and migration of gastrula cells and hindbrain motor neurons, affording effective movement towards their targets. Disruption of the *tri* homologue *Ltap* in Loop-tail mice results in severe spina bifida[17,32]. It will be important to determine whether neural tube closure defects are caused by disrupted gastrulation movements, or whether they reflect later *Ltap* functions in neurulation-specific cell behaviours.

There is considerable evidence that several Wnt signalling pathways, including canonical Wnt/β-catenin and non-canonical Wnt/calcium and PCP, regulate morphogenesis during vertebrate development[33]. Among these, the PCP pathway mediates mediolateral cell elongation that underlies convergence and extension movements[23,26,27]. Inhibition of convergence and extension movements in frog and fish embryos overexpressing *stbm* or injected with *stbm* MOs[8,9] suggests that Tri/Stbm is a mediator of tissue polarity. Our finding that inactivation of *tri* in zebrafish gastrulae impairs mediolateral cell elongation provides the first genetic evidence that homologous molecules underlie tissue polarity in flies and vertebrates. Genetic epistasis studies in *Drosophila* suggest that Stbm/Vang functions within, or parallel to, the Frizzled/PCP pathway[14]. In vertebrates, Tri/Stbm was shown to associate with Dsh *in vitro*, to recruit Dsh to the membrane *in vivo* and to promote c-Jun phosphorylation, suggesting that it functions as a positive component of PCP signalling[9]. Our results support the notion that the relationship between Tri/Stbm and the PCP pathway is not simply quantitative, but rather that Tri/Stbm modulates PCP signalling, perhaps functioning in a parallel pathway to control cell polarity underlying cell movements during gastrulation. It is possible that Tri/Stbm cooperates with a vertebrate homologue of the *Drosophila* Prickle protein in a feedback amplification mechanism similar to that proposed for wing tissue polarity[34]. However, the interaction between *stbm/vang* and *prickle* is complex and other data from *Drosophila* suggests these genes may be antagonists[6]. Moreover, our data suggests Tri/Stbm may mediate motor neuron migration independently of PCP signalling, thus providing an entry point to elucidate the molecular basis of this class of neuronal migration. This study underscores the complexity of genetic interactions Tri/Stbm engages in to establish tissue polarity and implicates this protein in the regulation of distinct movement behaviours during vertebrate development. □

Methods

Zebrafish maintenance and staging

Zebrafish embryos were produced by natural matings and adults maintained as described[1]. Embryo staging was performed according to morphology as described[35].

Genetic mapping and positional cloning

Detailed methods are described in Supplementary Information. The *stbm* coding sequence was amplified by reverse transcription (RT)-PCR from tri^{m209}, tri^{m747} and tri^{tc240a} homozygous mutant alleles and then directly sequenced.

Morpholino and RNA injections

Injections were performed at the one-cell stage as described[3,15]. The *stbm*/*tri* MO was obtained from Gene Tools, LLC (Philomath, OR), and was previously described[9]. The *tri*/*stbm* and mutated tri^{m747} open reading frames were subcloned into an expression vector and verified by sequencing. Sense-capped RNA was synthesized using mMessage mMachine (Ambion, Austin, TX) after template linearization. For phenotype rescue and phenocopy experiments, 5–50 pg *tri* RNA and 1–4 ng *tri* MO were used per embryo. Injection of greater than 8 ng of MO caused increasing central nervous system degeneration commonly observed with MO injections[15]. Embryos scored for suppression of the *tri* phenotype were genotyped by PCR using the simple sequence length polymorphism marker Z17411.

Immunostaining

Islet antibody staining and GFP imaging were performed as described[5] and phenylthiourea (0.003% w/v) was used to inhibit pigmentation. Expression of Myc-tagged Xdd1 was detected using an anti-Myc antibody (Calbiochem, San Diego, CA) as described[12], and imaged using a Zeiss LSM 510 laser scanning inverted confocal microscope (Zeiss, Thornwood, NY).

Transplantation experiments

To determine the autonomy of *tri* function during gastrulation, host embryos were injected with RNA encoding membrane-localized GFP[26] and donor embryos with rhodamine–dextran (Molecular Probes, Eugene, OR) and RNA encoding membrane GFP at the one-cell stage. Cells were extracted from donor embryos at the 1000-cell stage and injected close to the margin of dome stage hosts using standard methods[36]. At tailbud-2 somite stages, embryos were mounted in 1.5% methyl cellulose and imaged using a Zeiss LSM 510 confocal microscope. *z*-series images of donor-derived ectodermal cells were acquired at 2-μm intervals. Determination of cell orientation, LWR and statistical analyses were performed as described[27]. The cell-autonomy of *tri* function during motor neuron migration was determined as described[31].

Gastrula and neuronal cell movement analyses

Time-lapse analyses of lateral gastrula mesodermal cells were performed as described[24] and movie images were collected at 30-s intervals. LWRs were measured from single-frame Nomarski images using Object-Image (Norbert Vischer) and calculated using Microsoft Excel software. Statistical analyses were performed using Student's *t*-test. Our observations indicate that cell behaviours driving convergence and extension movements change continuously. Thus, our methods do not provide a comprehensive description of cell behaviours observed between 80% epiboly and the end of gastrulation. GFP-expressing motor neurons in wild-type and *tri* embryos were imaged at 200× magnification on an Olympus BX60 microscope (Melville, NY). Time-lapse recordings were made using Cytos software (Applied Scientific Instrumentation, Eugene, OR). Image processing and analysis was performed using DIAS software (Solltech, Iowa City, IA).

RECEIVED 17 MAY 2002; REVISED 6 JUNE 2002; ACCEPTED 6 JUNE 2002;
PUBLISHED 8 JULY 2002.

1. Solnica-Krezel, L. *et al. Development* **123,** 67–80 (1996).
2. Sepich, D. S. *et al. Genesis* **27,** 159–173 (2000).
3. Marlow, F. *et al. Dev. Biol.* **203,** 382–399 (1998).

4. Hammerschmidt, M. *et al. Development* **123,** 143–151 (1996).
5. Bingham, S., Higashijima, S., Okamoto, H. & Chandrasekhar, A. *Dev. Biol.* **242,** 149–160 (2002).
6. Taylor, J., Abramova, N., Charlton, J. & Adler, P. N. *Genetics* **150,** 199–210 (1998).
7. Wolff, T. & Rubin, G. M. *Development* **125,** 1149–1159 (1998).
8. Darken, R. S. *et al. EMBO J.* **21,** 976–985 (2002).
9. Park, M. & Moon, R. T. *Nature Cell Biol.* **4,** 20–25 (2002).
10. Haffter, P. *et al. Development* **123,** 1–36 (1996).
11. Driever, W. *et al. Development* **123,** 37–46 (1996).
12. Sokol, S. Y. *Curr. Biol.* **6,** 1456–1467 (1996).
13. Heisenberg, C. P. *et al. Nature* **405,** 76–81 (2000).
14. Adler, P. N. & Lee, H. *Curr. Opin. Cell Biol.* **13,** 635–640 (2001).
15. Nasevicius, A. & Ekker, S. C. *Nature Genet.* **26,** 216–220 (2000).
16. Heisenberg, C. P. & Tada, M. *Curr. Biol.* **12,** R126–R128 (2002).
17. Murdoch, J. N., Doudney, K., Paternotte, C., Copp, A. J. & Stanier, P. *Hum. Mol. Genet.* **10,** 2593–2601 (2001).
18. Park, M. & Moon, R. T. *Nature Cell Biol.* **4,** 467 (2002).
19. Lekven, A. C., Thorpe, C. J., Waxman, J. S. & Moon, R. T. *Dev. Cell* **1,** 103–114 (2001).
20. Erter, C. E., Wilm, T. P., Basler, N., Wright, C. V. & Solnica-Krezel, L. *Development* **128,** 3571–3583 (2001).
21. Wilson, S. W. & Rubenstein, J. L. *Neuron* **28,** 641–651 (2000).
22. Heisenberg, C. P. & Nusslein-Volhard, C. *Dev. Biol.* **184,** 85–94 (1997).
23. Marlow, F., Topczewski, J., Sepich, D. S. & Solnica-Krezel, L. *Curr. Biol.* **12,** 876–884 (2002).
24. Myers, D. C., Sepich, D. S. & Solnica-Krezel, L. *Dev. Biol.* **243,** 81–98 (2002).
25. Concha, M. L. & Adams, R. J. *Development* **125,** 983–994 (1998).
26. Wallingford, J. B. *et al. Nature* **405,** 81–85 (2000).
27. Topczewski, J. *et al. Dev. Cell.* **1,** 251–264 (2001).
28. Trinkaus, J. P. *J. Exp. Zool.* **281,** 328–335 (1998).
29. Chandrasekhar, A., Moens, C. B., Warren, J. T. Jr., Kimmel, C. B. & Kuwada, J. Y. *Development* **124,** 2633–2644 (1997).
30. Higashijima, S., Hotta, Y. & Okamoto, H. *J. Neurosci.* **20,** 206–218 (2000).
31. Moens, C. B. & Fritz, A. *Methods Cell Biol.* **59,** 253–272 (1999).
32. Kibar, Z. *et al. Nature Genet.* **28,** 251–255 (2001).
33. Peifer, M. & McEwen, D. G. *Cell* **109,** 271–274 (2002).
34. Tree, D. R. P. *et al. Cell* **109,** 371–381 (2002).
35. Kimmel, C. B., Ballard, W. W., Kimmel, S. R., Ullmann, B. & Schilling, T. F. *Dev. Dyn.* **203,** 253–310 (1995).
36. Westerfield, M. *The zebrafish book* (University Oregon Press, Eugene, 1995).

ACKNOWLEDGEMENTS

We thank B. Appel, R. Blakely, A. Schier, and C.V.E. Wright for critical comments. We thank J. Clanton and C. Baccam for excellent fish care, M. Halpern for γ-ray-mutagenized fish, M. Westerfield, H. Takeda, P. Ingham, M. Ekker, Y. Grinblat, B. Thisse, C. Thisse, E. Weinberg and T. Jowett for probes, R. Harland, S. Sokol and M. Tada for constructs, and C.-P. Heisenberg and H. Okamoto for fish. S.B. and A.C. are indebted to K. Cooper and C. Moens for invaluable guidance in transplantation procedures. The Zeiss confocal microscope is supported by National Insitutes of Health (NIH) grant 1S10RR015682. J.R.J. and D.S.S. are supported by a National Institutes of Health Vascular Biology Training Grant (T32HL07751). S.B. is supported by a NSF-Missouri's Alliance for Graduate Education and the Professoriate (MAGEP) fellowship and A.C. by NIH grant NS40449. L.S.K. is supported by NIH grant GM55101 and Pew Scholars Program in the Biomedical Sciences.
Correspondence and requests for material should be addressed to L.S.K
Supplementary Information is available on *Nature Cell Biology's* website (http://cellbio.nature.com).

COMPETING FINANCIAL INTERESTS

The authors declare that they have no competing financial interests.

Methods

Genetic mapping and positional cloning

To put *tri* on the genetic map, a genome scan was performed using the γ-irradiation-induced deletion allele *tri*^{v7} and a panel of 125 simple-sequence length polymorphism markers representing 25 linkage groups. The linkage group 7 marker Z9067 was absent in *tri*^{v7} embryos. Further genetic analysis on a panel of 50 *tri*^{m209} embryos linked *tri* to a cluster of four linkage group 7 markers, also deleted in *tri*^{v7} embryos (Supplementary Fig. S1). High-resolution mapping using Z17411 and a panel of 2,400 *tri*^{m209} and *tri*^{m747} embryos placed this marker less than 0.02 cM from the *tri* locus. The ends of BAC clones were sequenced directly and YAC ends recovered by self-circularization. BAC and YAC end sequencing uncovered polymorphic markers used to determine a critical interval for the *tri* locus. Sequencing of BAC137K24 identified a *stbm* homologue[1] located ~9 kb from Z17411.

Morpholino and RNA injections

For *tri* gain- and loss-of-function experiments, 50-300 pg *tri* RNA and 1-32 ng *tri* MO were used. The *dishevelled-ΔN*, *rho kinase 2* (*rok2*), and *dominant negative-rok2* constructs were previously described[2,3]. For epistatic analyses, doses of 30-100 pg *dishevelled-ΔN*, 60-180 *rok2*, 1-50 pg *dominant negative-rok2* , and 0.5-50 pg *tri* RNA were used. Doses of 1 pg-1 ng *tri* MO were used to "knock-down" *tri* function in *slb*^{zf216} embryos.

Whole-mount in situ hybridization and immunostaining

Antisense RNA probes *opl*[4], *krox-20* (ref. 5), *myoD*[6], *emx1* (ref. 7), *pax2b*[8], *hgg1* (ref. 9), *dlx3*[10], *shh*[11], and *deltaC*[12] were used for in situ hybridization as described[13]. To monitor rat Rok2 protein distribution, 50 pg of rat *rok2* RNA was injected alone, or with 200 pg *tri*, 60 pg *wnt11*, or *tri* plus *wnt11* RNA. Embryos were fixed and stained as described[14] using the following antibodies: primary C20 anti-Rok2 polyclonal antibody (1:100) (Research Antibodies) and anti-goat IgG secondary antibody conjugated to Alexa green 488 (1:250) (Molecular Probes). Images were acquired using a Zeiss LSM 510 laser scanning inverted confocal microscope.

1. Park, M. & Moon, R.T. *Nat. Cell Biol.* **4,** 20-25 (2002).
2. Tada, M. & Smith, J.C. *Development* **127,** 2227-2238 (2000).
3. Marlow, F., Topczewski, J., Sepich, D.S. & Solnica-Krezel, L. *Curr. Biol.* In Press (2002).
4. Grinblat, Y., Gamse, J., Patel, M. & Sive, H. *Development* **125,** 4403-4416 (1998).
5. Oxtoby, E. & Jowett, T. *Nucleic Acids Res.* **21,** 1087-1095 (1993).
6. Weinberg, E.S., *et al. Development* **122,** 271-280 (1996).
7. Morita, T., Nitta, H., Kiyama, Y., Mori, H. & Mishina, M. *Neurosci. Lett.* **198,** 131-134 (1995).
8. Krauss, S., Johansen, T., Korzh, V. & Fjose, A. *Development* **113,** 1193-1206 (1991).
9. Thisse, C., Thisse, B., Halpern, M.E. & Postlethwait, J.H. *Dev. Biol.* **164,** 420-429 (1994).
10. Akimenko, M.A., Ekker, M., Wegner, J., Lin, W. & Westerfield, M. *J. Neurosci.* **14,** 3475-3486 (1994).
11. Krauss, S., Concordet, J.P. & Ingham, P.W. *Cell* **75,** 1431-1444 (1993).
12. Haddon, C., *et al. Development* **125,** 359-370 (1998).
13. Thisse, C. & Thisse, B. in *Zebrafish Science Monitor* 8-9 (1998).
14. Topczewski, J., *et al. Dev. Cell.* **1,** 251-264 (2001).

Movies S1 and S2

These movies are continuous Nomarski time-lapse recordings (approximately 12 minutes) of mesodermal cells converging dorsally. (Movie S1) By the end of gastrulation (tailbud-1 somite), WT mesodermal cells in dorsolateral regions are elongated, closely packed, and move dorsally (to the right, in the movie) along straighter paths achieving greater net speeds compared to earlier gastrulation stages. (Movie S2) In contrast, by the end of gastrulation dorsolateral mesodermal cells in *tri* mutant embryos are not elongated and move more slowly towards dorsal while taking indirect paths.

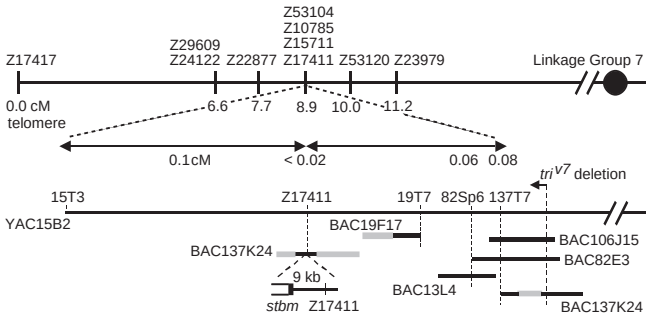

Figure S1 **Positional cloning of *tri*.** Integrated genetic and physical maps of the *tri* locus. The γ-irradiation-induced deletion allele *tri*^{v7} (breakpoint indicated) was used to map *tri* to linkage group 7. Linkage analysis placed marker Z17411 less than 0.02 cM from *tri*. Chimeric BACs 137K24 and 19F17 contained disparate genetic elements (indicated in grey) that did not map to this genetic region. Sequencing of BAC137K24 identified a *stbm* homologue located ~9 kb from Z17411. cM, centimorgan.

Movies S3 and S4

These movies are continuous time-lapse recordings of GFP-expressing facial (nVII) motor neurons acquired every 5 minutes for periods ranging from 4-8 hours. Images show dorsal views of the hindbrain with anterior to the left. In WT embryos (Movie S3), facial motor neurons are born in rhombomere 4 (center) and several cells migrate posteriorly toward rhombomeres 6 and 7. In *tri* mutant embryos (Movie S4), facial motor neurons are born in rhombomere 4 (center left). Mutant cells change their shapes frequently but do not migrate effectively toward rhombomeres 6 and 7.

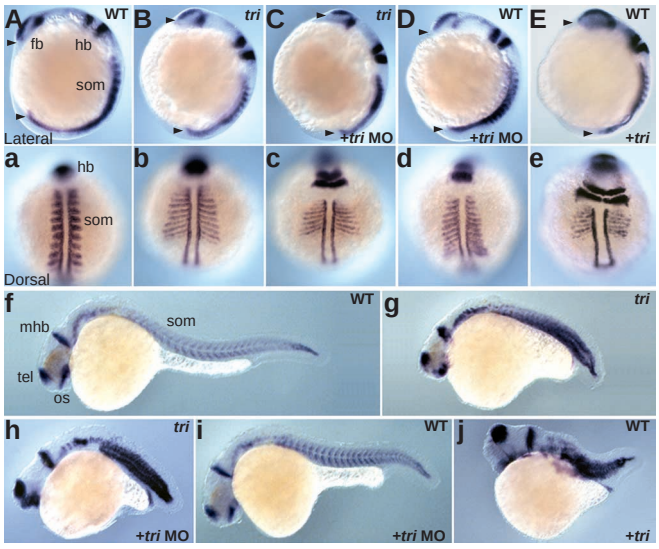

Figure S2 **Tri/Stbm does not regulate anteroposterior neural patterning. A,a-E,e,** Eight-ten somite embryos labeled with the forebrain marker *opl*, the hindbrain marker *krox-20*, and the somitic marker *myoD*. Arrowheads indicate anteroposterior length. WT (**A,a**) and *tri*^{m209} (**B,b**) embryos. *tri* (**C,c**) and WT (**D,d**) embryos injected with *tri* MO, and WT embryos (**E,e**) injected with *tri* RNA show inhibited convergence and extension, as evidenced by mediolaterally broadened *opl*, *krox-20*, and *myoD* domains but normal anteroposterior neural patterning. **f-j,** Lateral views of 1 day post-fertilization embryos labeled with *myoD* and the telencephalon marker *emx1* and the midbrain/hindbrain marker *pax2b*. WT (**f**) and *tri*^{m209} (**g**) embryos. *tri* (**h**) and WT (**i**) embryos injected with *tri* MO, and WT (**j**) embryos injected with *tri* RNA show essentially normal expression of neural markers. fb, forebrain; hb, hindbrain; som, somites; tel, telencephalon; mhb, midbrain/hindbrain boundary; os, optic stalks.

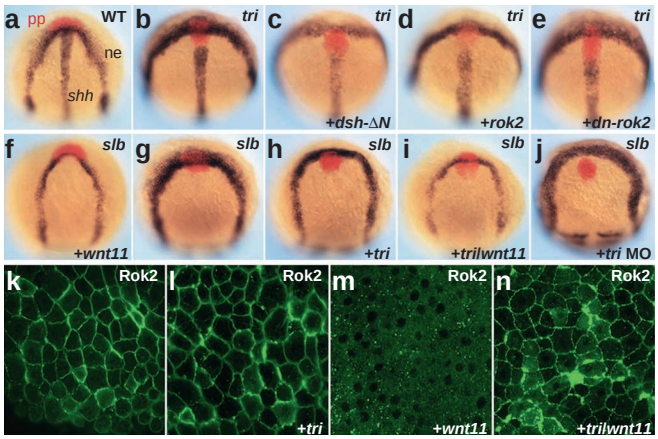

Figure S3 **Epistatic analysis of *tri* and PCP pathway components. a-e,** Two-three somite embryos labeled with the prechordal plate (pp) marker *hgg1* (red), *dlx3* marker delimiting the neuroectoderm (ne), and midline marker *shh*. WT (**a**) and *tri*^{m209} (**b**) embryos. Injection of *dishevelled-ΔN* (**c**), *rho kinase 2* (*rok2*) (**d**), or *dominant-negative rok2* (**e**) RNA did not suppress the *tri* convergence and extension phenotype. **f-j,** One-two somite *slb*^{tz216} embryos (verified by *deltaC* somitic staining, out of focus) labeled with *hgg1* (red) and *dlx3*. **f,** *slb*^{tz216} (*wnt11*) embryos rescued with *wnt11* RNA show *hgg1* staining anterior to a narrow *dlx3* domain. **g**, *slb*^{tz216} embryo. Injection of *tri* RNA (**h**), *tri* plus *wnt11* RNA (**i**), or low doses of *tri* MO (**j**) did not suppress the *slb* convergence and extension phenotype. **k-n,** Distribution of rat Rok2 upon overexpression in zebrafish blastulae was juxtamembranous when injected alone (**k**) or with *tri* RNA (**l**). Co-injection of *wnt11* with rat *rok2* removed Rok2 from the membrane (**m**) whereas co-injection of *rok2/wnt11* plus *tri* did not (**n**).